Asymptotic Analysis of the Structure of Moderately Rich Methane-Air Flames

K. SESHADRI,* X. S. BAI, H. PITSCH, and N. PETERS**
Institut für Technische Mechanik, RWTH Aachen, D-52056 Aachen, Federal Republic of Germany

The asymptotic structure of laminar, moderately rich, premixed methane flames is analyzed using a reduced chemical-kinetic mechanism comprising four global reactions. This reduced mechanism is different from those employed in previous asymptotic analyses of stoichiometric and lean flames, because a steady-state approximation is not introduced for CH_3. The aim of the present analysis is to develop an asymptotic model for rich flames, which can predict the rapid decrease of the burning velocity with increasing equivalence ratio ϕ. In the analysis, the flame structure is presumed to consist of three zones: a preheat zone with a normalized thickness of the order of unity, a thin reaction zone, and a postflame zone. The preheat zone is presumed to be chemically inert, and in the postflame zone the products are in chemical equilibrium and the temperature is equal to the adiabatic flame temperature T_b. In the reaction zone the chemical reactions are presumed to take place in two layers: the inner layer and the oxidation layer. The rate constants of these reactions are evaluated at T^0, which is the characteristic temperature at the inner layer. In the inner layer the dominant reactions taking place are those between the fuel and radicals, and between CH_3 and the radicals. An important difference between the structure of the inner layer of rich flames and that of lean flames analyzed previously is the enhanced influence of the chain-breaking reaction $CH_3 + H + (M) \rightarrow CH_4 + (M)$ in rich flames. Here M represents any third body. This reaction decreases the concentration of H radicals, which in turn decreases the values of the burning velocity. In the oxidation layer of rich flames, the reactive–diffusive balance of O_2 is considered. This differs from the structure of the oxidation layer of lean flames where the reactive–diffusive balance of H_2 and CO was of primary interest. The burning velocities calculated using the results of the asymptotic analysis agree reasonably well with the burning velocities calculated numerically using chemical-kinetic mechanisms made up of elementary reactions. The values of the characteristic temperature at the inner layer T^0 are found to increase with increasing values of the equivalence ratio and to approach T_b at $\phi = 1.36$. When T^0 is very close to T_b, the asymptotic analysis developed here is no longer valid and an alternative asymptotic analysis must be developed for even larger equivalence ratios. © 1998 by The Combustion Institute

INTRODUCTION

Reduced chemical-kinetic mechanisms have been employed successfully previously to analyze the asymptotic structure of laminar, stoichiometric, and lean methane flames [1–6]. For rich flames, these analyses did not predict the observed rapid decrease of the burning velocities with increasing equivalence ratio [1–6]. Here, an asymptotic analysis, which applies to rich, laminar methane flames, is developed.

Detailed and reduced chemical-kinetic mechanisms have been employed in previous numerical computations of the structure and burning velocities of stoichiometric, lean, and rich methane flames [7–10]. The reduced four-step mechanisms used in these analyses were deduced from detailed mechanisms after introducing steady-state approximations for a number of intermediate species, including CH_3, and radicals including OH and O but not H. The reaction rates of the global reactions in the reduced mechanisms were expressed in terms of the reaction rates of elementary steps. The main contributors to these global rates are called the principal reactions and the others, additional reactions. Among the additional reactions, the chain-breaking step $CH_3 + H + (M) \rightarrow CH_4 + (M)$ was found to have a significant influence on the burning velocities [8, 9]. Here M represents any third body. This reaction was found to decrease the burning velocities [8]. For stoichiometric, lean, and rich flames, a set of approximations have been described [9, 10], for which the numerically calculated values of the burning velocities obtained using the reduced mechanism agree well with those obtained using the

*Permanent address: Center for Energy and Combustion Research, Department of Applied Mechanics and Engineering Sciences, University of California at San Diego, La Jolla, California 92093-0411.
**Division of Fluid Mechanics, Department of Heat and Power Engineering, Lund Institute of Technology, S 221 00 Lund, Sweden.

COMBUSTION AND FLAME 113:589–602 (1998)
© 1998 by The Combustion Institute
Published by Elsevier Science Inc.
0010-2180/98/$19.00
PII S0010-2180(97)00272-1

detailed mechanisms and measurements. For stoichiometric and lean flames the burning velocities were found to increase with increasing values of the equivalence ratio ϕ. For moderately rich flames, with values of ϕ between 1.0 and 1.4, the burning velocities were found to decrease rapidly with increasing values of the equivalence ratio [9, 10]. For very rich flames, with values of ϕ greater than 1.4, the burning velocities were found to decrease slowly with increasing values of the equivalence ratio [10]. The profiles of temperature and of concentrations of reactants (CH_4 and O_2), products (H_2O and CO_2), intermediate species (H_2 and CO), and radicals (H, OH, and O) calculated using the reduced mechanisms were found to agree well with those obtained using the detailed mechanisms [9, 10]. The concentration profiles of CH_3 calculated using the reduced mechanisms were found to be significantly higher than those calculated using the detailed mechanisms [9, 10]. This indicates that the steady-state approximation for CH_3 is not accurate [10].

The asymptotic analysis of Peters and Williams [1] was performed with a reduced three-step mechanism deduced from a four-step mechanism after introducing a steady-state approximation for the H radical. Only the contributions of the principal elementary reactions to the rates of the global steps were considered in the analysis [1]. The asymptotic analyses of Seshadri and Peters [2], Seshadri and Göttgens [3], and Bui-Pham et al. [4] employed a four-step mechanism. These analyses treated the contribution of additional reactions, including the chain-breaking step $CH_3 + H + (M) \rightarrow CH_4 + (M)$, to the rates of the global steps as a perturbation and included only the leading order terms [2–4]. For ϕ greater than unity all asymptotic analyses failed to predict the observed rapid decrease of the burning velocities with increasing equivalence ratio. The analysis of Bui-Pham *et al*. [4] predicted only a weak decrease of the burning velocities with increasing equivalence ratio.

The aim of the present analysis is to develop an asymptotic model that can predict the rapid decrease of the burning velocities with increasing equivalence ratio. The analysis employs a reduced mechanism in which the intermediate species CH_3 is not presumed to maintain steady state. The contribution of the chain-breaking reaction $CH_3 + H + (M) \rightarrow CH_4 + (M)$ to the rates of the global reactions of the reduced mechanism is included in the analysis. The analysis developed here is valid for moderately rich flames. The results are not accurate for stoichiometric and lean flames and do not apply for very rich flames.

REDUCED CHEMICAL-KINETIC MECHANISM

Two sets of elementary chemical-kinetic mechanisms are assembled from Table 1.1 of Ref. 11, for describing the oxidation of methane. These mechanisms are called the C_3-mechanism and the C_1-mechanism. In the C_3-mechanism, reactions in which compounds made up of four or more carbon atoms participate, are not included. The C_3-mechanism also excludes reactions in which the species C_3H_7 and C_3H_8 appear and comprises steps 1–72 shown in Table 1.1 of Ref. 11. In the C_1-mechanism, reactions in which compounds made up of two or more carbon atoms participate are not included. The C_1-mechanism comprises reactions 1–35 and 37–40 shown in Table 1.1 of Ref. 11. The elementary step 36 is the reaction $CH_3 + CH_3 + (M) \rightarrow C_2H_6 + (M)$, which is neglected in the C_1-mechanism because it leads to the C_2-chain. The inclusion of this reaction, in general, decreases the overall chain-breaking effects of the C_1-mechanism in comparison with those in the C_3-mechanism and the C_2-mechanism [10] and therefore leads to slightly larger burning velocities. Around $\phi = 1.2$, the burning velocity calculated using the C_3-mechanism is approximately 12% larger than that calculated using the C_1-mechanism. The C_1-mechanism has been employed in previous numerical [7–10] and asymptotic studies [1–4] of premixed methane flames and provides sufficiently accurate values of the burning velocity even for moderately rich flames. The species CH_4, O_2, H_2O, CO_2, CH_3, CH_2, CH, CH_2O, CHO, CO, H_2, HO_2, O, OH, and H appear in this C_1-mechanism. In the C_3-mechanism, the species C_2H, C_2H_2, C_2H_3, C_2H_4, C_2H_5, C_2H_6, CHCO, C_3H_3, C_3H_4, C_3H_5, and C_3H_6 appear, in addition to those in the C_1-mechanism. The burning veloc-

ities calculated using the C_1-mechanism will be compared with those calculated using the C_3-mechanism.

A reduced five-step chemical-kinetic mechanism is deduced from the C_1-mechanism after introducing steady-state approximations for CH_2, CH, CH_2O, CHO, HO_2, O, and OH. This reduced five-step mechanism can be written as

$$CH_4 + H \rightleftharpoons CH_3 + H_2, \qquad (Ia')$$

$$CH_3 + H + H_2O \rightleftharpoons CO + 3H_2, \qquad (Ib')$$

$$CO + H_2O \rightleftharpoons CO_2 + H_2, \qquad (II')$$

$$H + H + M \rightleftharpoons H_2 + M, \qquad (III')$$

$$O_2 + 3H_2 \rightleftharpoons 2H + 2H_2O. \qquad (IV')$$

The global reactions Ia′ and Ib′ are chain breaking and represent the reactions between the fuel and the radicals and between CH_3 and the radical to form CO and H_2. The global reaction II′ represents the oxidation of CO to form the final product CO_2. The global reaction III′ represents the three-body recombination steps and is also responsible for a major fraction of heat released in the flame. The global reaction IV′ represents the reaction of O_2 with the radicals and the formation of H_2O. It comprises the chain-branching steps. This five-step mechanism was employed in a previous numerical study of the structure of nonpremixed methane flames [12]. Table 1 shows the elementary reactions that are presumed to be the major contributors to the rates of the global steps of the reduced mechanism and includes the chain-breaking step 34. The symbols f and b appearing in the first column of Table 1, respectively, identify the forward and backward steps of a reversible elementary reaction n. The backward steps of reactions 5, 34, 35, and 38 are neglected. The elementary reactions are identified using the same numbers as those shown in Table 1.1 of Ref. 11. The reaction rate coefficient k_n of the elementary reactions is calculated using the expression $k_n = B_n T^{\alpha_n} \exp[-E_n/(\hat{R}T)]$, where T denotes the temperature and $\hat{R}$ is the universal gas constant. The quantities B_n, α_n, and E_n are the frequency factor, the temperature exponent, and the activation energy of the elementary reaction n, respectively. The concentration of the third-body C_M is calculated using the relation $C_M = [p\bar{W}/(\hat{R}T)]\Sigma_{i=1}^{n} \eta_i Y_i/W_i$ where p denotes the pressure; $\bar{W}$ is the average molecular weight; and Y_i, W_i, and η_i, are, respectively, the mass fraction, the molecular weight, and the chaperon efficiency of species i. The chaperon efficiencies are shown in Table 1. The asymptotic analysis is performed using only the elementary reactions shown in Table 1.

In the analysis, a steady-state approximation is introduced for H radicals [1]. This gives a four-step mechanism that can be written as

$$CH_4 + 0.5\,O_2 + 0.5\,H_2 \rightleftharpoons CH_3 + H_2O, \qquad (Ia)$$

$$CH_3 + 0.5\,O_2 \rightleftharpoons CO + 1.5\,H_2, \qquad (Ib)$$

$$CO + H_2O \rightleftharpoons CO_2 + H_2, \qquad (II)$$

$$O_2 + 2\,H_2 \rightleftharpoons 2\,H_2O. \qquad (III)$$

The reaction rates of the global steps w_k, in the five-step mechanism (k = Ia–IV′), and in the four-step mechanism (k = Ia–III), expressed in terms of the reaction rates of elementary reactions w_n are

$$\left.\begin{aligned} w_{Ia'} &= w_{Ia} = w_{38} - w_{34},\\ w_{Ib'} &= w_{Ib} = w_{35},\\ w_{II'} &= w_{II} = w_{18f} - w_{18b},\\ w_{III'} &= w_{III} = w_5 + w_{34},\\ w_{IV'} &= w_{1f} - w_{1b}. \end{aligned}\right\} \qquad (1)$$

In the four-step mechanism Ia–III, if a steady-state approximation is introduced for CH_3, then the global step Ib will disappear and the global fuel-consumption reaction $CH_4 + O_2 \rightleftharpoons CO + H_2 + H_2O$, deduced from Ia and Ib, will replace Ia. The reaction rate of this global fuel-consumption step is given by w_{Ia}. This approximation was employed in previous asymptotic analysis of stoichiometric and lean methane flames [1–6]. In rich flames the concentration of O atoms can be expected to be lower than that in lean flames. Hence O atoms are expected to have a greater influence on the structure of rich flames in comparison with their influence on the structure of lean flames. Equation 1 shows that the reaction rate of the global step Ib is given by w_{35}, which is proportional to the concentration of O atoms (see Table 1). Therefore the present formulation, in which a

TABLE 1

Rate Data for Elementary Reactions Employed in Asymptotic Analysis

Number	Reaction	B_n	α_n	E_n
1f	$O_2 + H \rightarrow OH + O$	2.000E+14	0.00	70.30
1b	$O + OH \rightarrow H + O_2$	1.568E+13	0.00	3.52
2f	$H_2 + O \rightarrow OH + H$	5.060E+04	2.67	26.3
2b	$H + OH \rightarrow O + H_2$	2.222E+04	2.67	18.29
3f	$H_2 + OH \rightarrow H_2O + H$	1.000E+08	1.60	13.80
3b	$H + H_2O \rightarrow OH + H_2$	4.312E+08	1.60	76.46
4f	$OH + OH \rightarrow H_2O + O$	1.500E+09	1.14	0.42
4b	$O + H_2O \rightarrow OH + OH$	1.473E+10	1.14	71.09
5[a]	$H + O_2 + M \rightarrow HO_2 + M$	2.300E+18	−0.80	0.00
18f	$CO + OH \rightarrow CO_2 + H$	4.400E+06	1.50	−3.10
18b	$H + CO_2 \rightarrow OH + CO$	4.956E+08	1.50	89.76
34[b]	$CH_3 + H \rightarrow CH_4$ k_0	6.257E+23	−1.80	0.00
	k_∞	2.108E+14	0.00	0.00
35	$CH_3 + O \rightarrow CH_2O + H$	7.000E+13	0.00	0.00
38	$CH_4 + H \rightarrow CH_3 + H_2$	2.200E+04	3.00	36.60

Units are moles, cubic centimeters, seconds, kJoules, Kelvin.

[a] Third body collision efficiencies are $[M] = 6.5[CH_4] + 1.5[CO_2] + 0.75[CO] + 0.4[N_2] + 6.5[H_2O] + 0.4[O_2] + 1.0$ [other].

[b] For reaction 34: $k = Fk_\infty k_0[p/(\hat{R}T)]/\{k_\infty + k_0[p/(\hat{R}T)]\}$, where $\log_{10} F = \log_{10} F_c/\{1 + (\log_{10}(k_0[p/(\hat{R}T)]/k_\infty)/\hat{N})^2\}$, $\hat{N} = 0.75 - 1.27 \log_{10} F_c$, and $F_c = 0.577 \exp[-T/2370.0]$.

steady-state approximation is not introduced for CH_3, directly includes the influence of O atoms on fuel-consumption through CH_3.

To simplify the calculation of the reaction rates of the global steps, the elementary reactions 2 and 3 are presumed to maintain partial equilibrium. Previous numerical calculations show that these approximations are reasonably accurate [10]. These approximations give the results

$$C_{OH} = [C_{H_2O}/(K_3 C_{H_2})]C_H,$$
$$C_O = [C_{H_2O}/(K_2 K_3 C_{H_2}^2)]C_H^2, \tag{2}$$

where C_i is the molar concentration of species i, and K_n is the equilibrium constant of the elementary step n. Also from the chemical-kinetic mechanism shown in Table 1 it follows that $K_4 = K_3/K_2$.

FORMULATION

The four-step mechanism Ia–III is used in the asymptotic analysis. The steady propagation of a planar, laminar flame under adiabatic and isobaric (small Mach number) conditions is considered. The solution to the equation of mass conservation is $\rho v = \rho_u s_L$, where ρ is the density, v the gas velocity, s_L the burning velocity, and subscript u refers to the initial conditions in the unburnt reactant mixture. The Lewis numbers for species i are assumed to be constants and defined as $\mathrm{Le}_i = \lambda/(\rho c_p D_i)$, where λ is the thermal conductivity, c_p the mean specific heat at constant pressure, and D_i the diffusion coefficient of species i. The diffusion velocity of the species is presumed to be given by Fick's Law [13]. The nondimensional species balance equations and the energy conservation equation can be written as

$$\frac{dX_i}{dx} - \frac{1}{\mathrm{Le}_i}\frac{d^2X_i}{dx^2} = \sum_{k=\mathrm{Ia}}^{\mathrm{III}} (\nu_{i,k}\omega_k), \qquad \frac{d\tau}{dx} - \frac{d^2\tau}{dx^2} = \sum_{k=\mathrm{Ia}}^{\mathrm{III}} (Q_k\omega_k), \tag{3}$$

where $x \equiv \int_0^{x'} (\rho v c_p/\lambda)\, dx'$ and x' is the spatial coordinate. The origin $x = 0$ is taken to coincide with the location of the inner reactive–diffusive zone. The quantity $\nu_{i,k}$ is the stoichiometric coefficient of species i in the global step k of the reduced mechanism. The value of $\nu_{i,k}$ is positive if species i appears on the right side of

global step k and negative if it appears on the left side. If the balance equation for each species is integrated, then the product of the mass fraction of the species with its diffusion velocity summed over all species will vanish only when Le_i is unity for all species [7]. A correction velocity is often introduced so that this sum will vanish [7]. For methane flames, Le_i for the reactants (CH_4 and O_2) and the major products (H_2O and CO_2) are very close to unity, and the mass fractions of the intermediate species are of lower order than those for the reactants and the products. Hence the correction velocity will be very small and is neglected in the asymptotic analysis.

The dependent variables X_i and τ are defined as

$$X_i \equiv \frac{Y_i W_{\mathrm{F}}}{Y_{\mathrm{Fu}} W_i}, \qquad \tau \equiv \frac{T - T_u}{T_c - T_u}, \tag{4}$$

where X_i is the normalized mass fraction of species i and τ the normalized temperature. Y_{Fu} is the initial value of Y_{F} in the unburnt reactant mixture, T_c is the temperature for "complete combustion," which is defined as the temperature in the burnt gas if the products are only CO_2, H_2O, and fuel CH_4 for $\phi > 1$, and subscript F refers to the fuel. From Eq. 4 it follows that $C_i = (\rho Y_{\mathrm{Fu}}/W_{\mathrm{F}})X_i$. The nondimensional reaction rates ω_k and heats of reaction Q_k are defined as

$$\omega_k \equiv \frac{\lambda W_{\mathrm{F}} w_k}{c_p Y_{\mathrm{Fu}} \rho_u^2 s_L^2}, \qquad Q_k \equiv \frac{Y_{\mathrm{Fu}}(-\Delta H_k)}{c_p (T_c - T_u) W_{\mathrm{F}}}, \tag{5}$$

where $(-\Delta H_k)$ is the heat release in the global step k. From the definition of Q_k it follows that $Q_{\mathrm{Ia}} + Q_{\mathrm{Ib}} + Q_{\mathrm{II}} + Q_{\mathrm{III}} = 1$.

The asymptotic structure of rich methane flames analyzed here is presumed to be similar to the structure of stoichiometric and lean flames analyzed previously [1–3]. The outer structure of the premixed flame is presumed to comprise an inert preheat zone of thickness of the order of unity, a thin reaction zone where all chemical reactions take place, and a postflame zone where the products are in equilibrium and the temperature is equal to its adiabatic value T_b. The reaction zone comprises the inner layer and the oxidation layer [1–6]. The preheat zone is located upstream of the reaction zone and the postflame zone downstream of the reaction zone. For given initial values of the equivalence ratio ϕ, the pressure p, the mass fractions of the reactants Y_{iu}, and the temperature T_u, the values of T_c and T_b and the mass fractions of the equilibrium products Y_{ib}, can be calculated. The equivalence ratio is given by the expression $\phi = n_{st} Y_{\mathrm{Fu}}/Y_{\mathrm{O_2u}}$, where n_{st} is the ratio of the mass of oxygen to the mass of fuel in a stoichiometric mixture of these reactants. For methane flames $n_{st} = 4$. The equilibrium products in the postflame zone are presumed to comprise CO_2, H_2O, O_2, CO, H_2, and N_2. Figure 1 shows values of Y_{ib} for rich mixtures of methane, oxygen, and nitrogen calculated for $T_u = 300$ K, $p = 1$ bar, and various values of ϕ. Figure 2 shows values of T_c and T_b calculated for $T_u = 300$ K, $p = 1$ bar, and various values of ϕ. Figure 2 also shows the values of the characteristic temperature at the inner layer T^0. The procedure employed to calculate T^0 is described later.

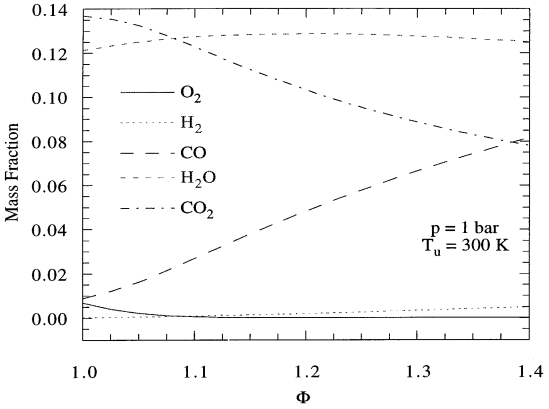

Fig. 1. Equilibrium mass fractions of the products Y_{ib}, as functions of equivalence ratio ϕ calculated for $T_u = 300$ K and $p = 1$ bar.

In the preheat zone the normalized mass fractions of CH_4, O_2, CO_2, and H_2O are of the order of unity. To leading order the profiles of these species can be calculated by neglecting the reaction terms in the balance equations. The profiles of CH_4 and O_2 in the preheat zone are

$$X_{\mathrm{F}} = 1 - \exp(\mathrm{Le}_{\mathrm{F}}\, x),$$

$$X_{\mathrm{O_2}} = X_{\mathrm{O_2u}} - (X_{\mathrm{O_2u}} - X_{\mathrm{O_2b}}) \exp(\mathrm{Le}_{\mathrm{O_2}}\, x) \tag{6}$$

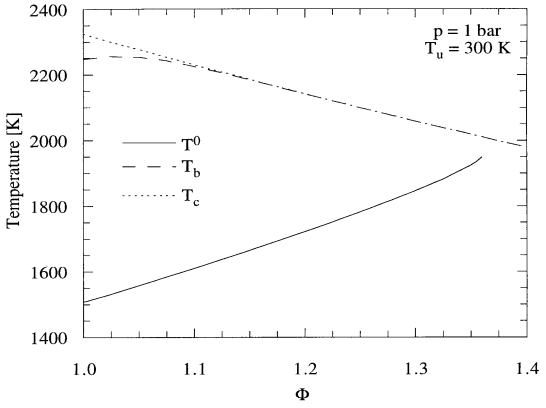

Fig. 2. Temperature for complete combustion T_c, equilibrium temperature in postflame zone T_b, and characteristic temperature at the inner layer T^0, as functions of the equivalence ratio ϕ calculated for $p = 1$ bar and $T_u = 300$ K.

where X_{O_2u} is the initial value of X_{O_2} in the unburnt reactant mixture, and X_{O_2b} the value in the postflame zone.

A schematic illustration of the structure of the preheat zone and the structures of the inner layer and the oxidation layer in the reaction zone are shown in Fig. 3. To illustrate the main qualitative features of the flame structure, sketches of the temperature profile and the concentration profiles of CH_4, CH_3, O_2, and H_2 are shown. The characteristic nondimensional thickness of the inner layer is presumed to be of order of δ and in this layer the reactions taking place at appreciable rates are the global steps Ia and Ib. The fuel is consumed in the inner layer,

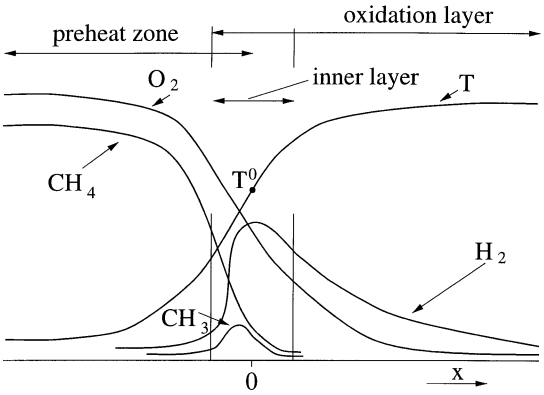

Fig. 3. Illustration of presumed asymptotic structure of preheat zone and reaction zone of premixed methane flames. Reaction zone shows inner layer and oxidation layer.

and the intermediate species CH_3 is produced and completely consumed in this layer. The characteristic nondimensional thickness of the oxidation layer is presumed to be of the order of ε and in this layer the global reactions II and III take place, and the rates of the global reactions Ia and Ib are presumed to be negligibly small. Oxygen is consumed in this layer. In the oxidation layer the global reaction II is presumed to maintain partial equilibrium everywhere except in a thin sublayer. The nondimensional thickness of this sublayer is presumed to be of the order of ν [1, 2]. In the analysis it is presumed that $\delta \ll \nu \ll \varepsilon \ll 1$. The validity of the presumed ordering is checked later using the results of the analysis.

Within the reaction zone the coordinate is selected such that the inner layer is located at $x = 0$, and the conditions there are identified by the superscript 0. The quantity T^0 shown in Fig. 3 is the characteristic temperature at the inner layer. In the asymptotic analysis of the reaction zone, the convective terms in the species balance equations and in the energy conservation equation shown in Eq. 3 are neglected because they are presumed to be small in comparison with the diffusive terms and the reactive terms. The activation energies of all the elementary reactions that appear in the global rates shown in Eq. 1 are small. Therefore in the asymptotic analysis the values of the rate constants of the elementary reactions are evaluated at T^0. Changes in the values of the rate constants with changes in the values of T are neglected [1, 2, 4]. In the asymptotic analysis of the reaction zone, the concentrations of H_2O and CO_2 are treated as being of the order of unity. To the leading order the values of X_{H_2O} and X_{CO_2} are presumed to be equal to their values in the postflame zone represented by X_{H_2Ob} and X_{CO_2b}, respectively. Also, in the reaction zone the concentrations of O_2, CO, and H_2 are presumed to be of the order of ε, and the concentration of CH_4 of the order of δ.

ASYMPTOTIC ANALYSIS OF THE INNER LAYER

The analysis of the structure of the inner layer is different from that of stoichiometric and lean

methane flames, because for rich flames a steady-state approximation is not introduced for CH_3. The balance equations for CH_4 and CH_3 obtained from Eq. 3 and using Eqs. 1, 2, and 4 are

$$\left.\begin{aligned}\frac{1}{\mathrm{Le_F}}\frac{d^2X_\mathrm{F}}{dx^2} &= \omega_{38}-\omega_{34},\\ \frac{1}{\mathrm{Le_{CH_3}}}\frac{d^2X_{\mathrm{CH_3}}}{dx^2} &= -\omega_{38}+\omega_{34}+\omega_{35}.\end{aligned}\right\} \tag{7}$$

The balance equation for CH_3 shows the formation of this compound by reaction 38 and consumption by the competing reactions 34 and 35. If reaction 34 is neglected and CH_3 is assumed to maintain steady state, a formulation equivalent to that employed in previous analyses [1–6] of stoichiometric and lean flames is recovered.

The diffusivities of CH_4 and CH_3 are nearly equal. Therefore, for simplicity the approximation $\mathrm{Le_F} \approx \mathrm{Le_{CH_3}}$ is used. For convenience, the definition $X_s = X_\mathrm{F} + X_{\mathrm{CH_3}}$ is introduced, and from Eq. 7 the differential equation

$$\frac{1}{\mathrm{Le_F}}\frac{d^2X_s}{dx^2} = \omega_{35} \tag{8}$$

is obtained. This shows that the sum of CH_4 and CH_3 is consumed eventually by reaction 35, which therefore is the rate determining step of fuel consumption in moderately rich methane flames. The rates of the elementary reactions 38 and 34 are very fast. The small fractional differences between these large quantities are presumed to be of the same order as the other terms in Eq. 7. Because of this the approximation $\omega_{38} \approx \omega_{34}$ is introduced. It gives the result $X_\mathrm{F} = (k_{34}/k_{38})X_{\mathrm{CH_3}}$. This is similar to the criterion employed by introducing a partial equilibrium approximation for a reversible elementary reaction [13, 14]. Here it is applied to two irreversible reactions. For large values of the ratio k_{34}/k_{38}, the approximate results

$$X_\mathrm{F} = X_s, \qquad X_{\mathrm{CH_3}} = (k_{38}/k_{34})X_s \tag{9}$$

are obtained. This approximation will be used in the analysis.

To calculate the source terms in Eq. 8, it is necessary to relate the concentration of H radicals to the concentration of the species appearing in the four-step mechanism Ia–III. The steady-state concentration of H can be calculated from the algebraic relation $\omega_{\mathrm{Ia}'} + \omega_{\mathrm{Ib}'} + 2\omega_{\mathrm{III}'} - 2\omega_{\mathrm{IV}'} = 0$ which gives the quadratic equation

$$\frac{X_\mathrm{H}^2}{R^2} + \frac{1}{\sigma}\left(\frac{k_{38}X_s}{k_{1f}X_{\mathrm{O_2}}}\right)\frac{X_\mathrm{H}}{R} + \frac{k_{34}k_{38}X_s}{k_{1f}k_{34}X_{\mathrm{O_2}}} + \kappa - 1 = 0 \tag{10}$$

where Eqs. 1, 2, 4, and 9 have been used. The quantities R, σ, and κ appearing in Eq. 10 are defined as

$$\left.\begin{aligned}R &= \frac{K_1^{0.5}K_2^{0.5}K_3X_{\mathrm{H_2}}^{1.5}X_{\mathrm{O_2}}^{0.5}}{X_{\mathrm{H_2O}}},\\ \sigma &= \frac{2k_{34}K_2^{0.5}X_{\mathrm{H_2}}^{0.5}}{k_{35}K_1^{0.5}X_{\mathrm{O_2}}^{0.5}},\\ \kappa &= \frac{k_5C_M}{k_{1f}}.\end{aligned}\right\} \tag{11}$$

The third term appearing on the left side of Eq. 10, $k_{34}k_{38}X_s/(k_{1f}k_{34}X_{\mathrm{O_2}})$, is deduced from the reaction rate of the chain-breaking step 34, $CH_3 + H + (M) \rightarrow CH_4 + (M)$. This term decreases the steady-state value of the H radicals. Equation 10 shows that X_H must be of the order of R. The value of κ is found to be small when it is evaluated at typical temperatures of the inner layer, therefore it is neglected. To analyze the structure of the inner layer, the expansions

$$x = \delta\zeta, \quad X_s = \delta\,\mathrm{Le_F}\,y_s, \quad X_{\mathrm{O_2}} = X_{\mathrm{O_2}}^0 + \delta y_{\mathrm{O_2}},$$
$$X_{\mathrm{H_2}} = X_{\mathrm{H_2}}^0 + \delta y_{\mathrm{H_2}} \tag{12}$$

are introduced, where the expansion parameter δ is presumed to be small. In this layer the quantities $\zeta, y_s, y_{\mathrm{O_2}}$, and $y_{\mathrm{H_2}}$ are treated as being of order of unity, $X_{\mathrm{O_2}}^0$ and $X_{\mathrm{H_2}}^0$ are of the order of ε and represent the leading order values of $X_{\mathrm{O_2}}$ and $X_{\mathrm{H_2}}$ at the inner layer. The values of $X_{\mathrm{O_2}}^0$ and $X_{\mathrm{H_2}}^0$ are obtained later. The small parameter δ is chosen such that

$$\delta = \frac{2k_{1f}^0k_{34}^0(K_2^0X_{\mathrm{H_2}}^0X_{\mathrm{O_2}}^0)^{0.5}}{k_{35}^0k_{38}^0(K_1^0)^{0.5}\,\mathrm{Le_F}}. \tag{13}$$

where the superscript 0 over any rate constant and equilibrium constant implies that its value is

evaluated at $T = T^0$. The value of T^0 is obtained later.

If the expansion for X_s given by Eq. 12 is introduced into Eq. 10 and Eq. 13 is used, the steady-state concentration of H radicals in the inner layer is given by

$$X_{\mathrm{H}} = 0.5R^0[-y_s + \sqrt{y_s^2 + 4(1 - \sigma^0 y_s)}]. \quad (14)$$

The quantities σ^0 and R^0 are the values of σ and R evaluated from Eq. 11 with the rate and equilibrium constants evaluated at T^0, and with X_{O_2} and X_{H_2} replaced by $X^0_{\mathrm{O}_2}$ and $X^0_{\mathrm{H}_2}$. Introducing Eq. 12 into Eq. 8 and using Eqs. 9, 11, and 14, the differential equation

$$\frac{d^2y_s}{d\zeta^2} = Ly_s(X_{\mathrm{H}}/R^0)^2, \quad (15)$$

is obtained, where

$$\left.\begin{aligned} L &= \frac{Ak^0_{35}k^0_{38}K^0_1K^0_3\,\mathrm{Le}_{\mathrm{F}}\,X^0_{\mathrm{O}_2}X^0_{\mathrm{H}_2}\delta^2}{k^0_{34}X_{\mathrm{H_2Ob}}}, \\ A &= \frac{Y_{\mathrm{Fu}}}{s_L^2W_{\mathrm{F}}}\left(\frac{\lambda^0}{c_p^0}\right)\left(\frac{\rho^0}{\rho_u}\right)^2, \end{aligned}\right\} \quad (16)$$

The quantity L is equivalent to a reduced Damköhler number and is presumed to be of order unity. Equation 16 explicitly relates s_L to the rate constant of the elementary reaction 34 and shows the influence of this reaction on the burning velocity. Boundary conditions for Eq. 15 must be obtained by matching the profile of X_s in the inner layer with its profile in the preheat zone as $\zeta \to -\infty$ and with its profile in the oxidation layer as $\zeta \to \infty$. In the preheat zone the concentration of CH_4 is given by Eq. 6. The value and derivative of X_{CH_3} with respect to x in the preheat zone is of the order of δ. Matching these solutions with the expansion for X_s shown in Eq. 12, it follows that as $\zeta \to -\infty$, $dy_s/d\zeta = -1$. Equation 14 shows that the concentration of the radicals becomes equal to zero when $y_s = 1/\sigma^0$. Upstream from this point the flow field is chemically inert because radicals are not present, and the profile of the fuel in the inner layer must match with its profile in the preheat zone. It follows that the matching conditions can be applied at $\zeta = -1/\sigma^0$ and at this point $dy_s/d\zeta = -1$ and $y_s = 1/\sigma^0$. In the oxidation layer the concentrations of CH_4 and CH_3 are negligibly small. Hence it follows that as $\zeta \to \infty$, $y_s = dy_s/d\zeta = 0$.

Integrating Eq. 15 once after treating y_s as the independent variable and $dy_s/d\zeta$ as the dependent variable and using the definition $y = \sigma^0 y_s$ and the matching conditions, the result

$$L = (\sigma^0)^2\left\{\int_0^1 y\left[\frac{y^2}{(\sigma^0)^2} + 2(1-y) - \frac{y}{\sigma^0}\left[\frac{y^2}{(\sigma^0)^2} + 4(1-y)\right]^{0.5}\right]dy\right\}^{-1} \quad (17)$$

is obtained. Equation 17 is evaluated numerically.

The results obtained in this section can be used to calculate s_L from Eq. 16 if the values of T^0, $X^0_{\mathrm{O}_2}$, and $X^0_{\mathrm{H}_2}$ are known. These quantities can be obtained by analyzing the structure of the oxidation layer.

ASYMPTOTIC ANALYSIS OF THE OXIDATION LAYER

In the oxidation layer the concentrations of CH_4 and CH_3 are negligibly small, and the influence of the overall steps Ia and Ib on the structure of this layer can be neglected. In this layer O_2, H_2, and CO are consumed by the overall steps II and III. The structure of the oxidation layer of rich flames can be expected to be influenced mainly by the consumption of O_2, represented by the overall step III, because the amounts of oxygen in rich flames are lower than those in lean flames. In previous asymptotic analyses of stoichiometric and lean flames, the structure of the oxidation layer was presumed to be influenced mainly by the oxidation of H_2 and CO [1–6]. Following previous analyses [1, 2, 5, 6], the water–gas shift reaction II is presumed to maintain partial equilibrium everywhere except in a thin sublayer within the oxidation layer, located immediately downstream of the inner layer. The structure of the oxidation layer is first analyzed with overall step II in partial equilibrium, followed by an analysis of the sublayer where the water–gas shift reaction is not in equilibrium.

Partial equilibrium for overall step II gives

$$X_{CO}/\mathrm{Le}_{CO} = \alpha(X_{H_2}/\mathrm{Le}_{H_2}), \tag{18}$$

where the quantity α is presumed to be of the order of unity and is defined as

$$\alpha = K_3^0 X_{CO_{2b}} \mathrm{Le}_{H_2}/(K_{18}^0 X_{H_2Ob} \mathrm{Le}_{CO}). \tag{19}$$

The differential equations describing the structure of this layer deduced from Eq. 3 are

$$\left.\begin{aligned} &\frac{1}{\mathrm{Le}_{O_2}}\frac{d^2X_{O_2}}{dx^2} = \omega_{III},\\ &\frac{d^2}{dx^2}\left[(1+\alpha)\frac{X_{H_2}}{\mathrm{Le}_{H_2}} - 2\frac{X_{O_2}}{\mathrm{Le}_{O_2}}\right] = 0,\\ &\frac{d^2}{dx^2}\left[(Q_{III}+2Q_{II})\frac{X_{O_2}}{\mathrm{Le}_{O_2}} - Q_{II}\frac{X_{H_2}}{\mathrm{Le}_{H_2}} + \tau\right] = 0. \end{aligned}\right\} \tag{20}$$

The value of $Q_{III} = 0.6232$ and that of $Q_{II} = 0.0363$. Since the value of Q_{II} is small it is neglected, and for convenience the definition $q = Q_{III}$ is introduced. The expansions

$$\left.\begin{aligned} &qx = \varepsilon\eta, \qquad qX_{O_2} = \varepsilon\,\mathrm{Le}_{O_2}(a+z),\\ &q(1+\alpha)X_{H_2} = 2\varepsilon\,Le_{H_2}(b+z), \tau = \tau_b - \varepsilon z, \end{aligned}\right\} \tag{21}$$

are introduced, where ε is a small expansion parameter and the quantities η, z, $\tau_b = (T_b - T_u)/(T_c - T_u)$, $a = qX_{O_2b}/(\varepsilon\,\mathrm{Le}_{O_2})$, and $b = q(1+\alpha)X_{H_2b}/(2\varepsilon\,\mathrm{Le}_{H_2})$ are treated as being of order unity. The presumed ordering of the quantities a and b implies that X_{O_2b} and X_{H_2b} are of order ε. The expansions for X_{H_2} and τ in Eq. 21 are written such that they satisfy the coupling relation in Eq. 20 and match with the temperature profile and concentration profiles in the postflame zone. From Eq. 10 it follows that in the oxidation layer the steady-state concentration of H radicals is given by $X_H = R$. The source term ω_{III} written in terms of the expansions shown in Eq. 21 after using Eqs. 1, 4, 5, and 11 is

$$\omega_{III} = qD_{III}\varepsilon^3(a+z)^{1.5}(b+z)^{1.5}, \tag{22}$$

where D_{III} is a characteristic Damköhler number and is given by

$$D_{III} = \frac{2^{1.5}Ak_5^0C_M^0(K_1^0K_2^0)^{0.5}K_3^0\,\mathrm{Le}_{H_2}^{1.5}\,\mathrm{Le}_{O_2}^{1.5}}{(1+\alpha)^{1.5}q^4X_{H_2Ob}}, \tag{23}$$

where C_M^0 is the value of C_M evaluated at $T = T^0$. The small expansion parameter is chosen such that

$$\varepsilon = D_{III}^{-0.25}. \tag{24}$$

Using Eqs. 21, 22, and 24 in Eq. 20 the differential equation

$$d^2z/d\eta^2 = (a+z)^{1.5}(b+z)^{1.5} \tag{25}$$

is obtained. Boundary conditions for Eq. 25 must be obtained by matching the profile of oxygen in this layer with its profile in the other reaction layers at $\eta = 0$, and with its profile in the postflame zone in the limit $\eta \to \infty$. In all layers except the oxidation layer, if the influence of reaction III on the structure of these layers is neglected, then from Eq. 3 the coupling relation $d^2(2X_F/\mathrm{Le}_F + X_{CH_2}/\mathrm{Le}_{CH_3} - 2X_{O_2}/\mathrm{Le}_{O_2})/dx^2 = 0$ is obtained. Integrating this coupling relation once and matching the result with the profiles of X_F and X_{O_2} in the preheat zone given by Eq. 6, the result $d(2X_F/\mathrm{Le}_F + X_{CH_2}/\mathrm{Le}_{CH_3} - 2X_{O_2}/\mathrm{Le}_{O_2})/dx = -2(1 - X_{O_2u} + X_{O_2b})$ is obtained. The quantity X_{O_2b} can be neglected because it is of order ε and very small for rich flames. Matching this result with the expansion for X_{O_2} in Eq. 21, the boundary condition

$$dz/d\eta = -(X_{O_2u} - 1) \tag{26}$$

is obtained at $\eta = 0$. Values of the initial concentration of oxygen in the range $1 < X_{O_2u} < 2$ are considered here. For methane flames at $X_{O_2u} = 1$, $\phi = 2$ and at $X_{O_2u} = 2$, $\phi = 1$. Matching the expansion for X_{O_2} in Eq. 21 with the profile of oxygen in the postflame zone the result $z = dz/d\eta = 0$ is obtained as $\eta \to \infty$. Using these matching conditions, Eq. 25 can be written as

$$2\int_0^{z^0}(a+z)^{1.5}(b+z)^{1.5}\,dz = (X_{O_2u} - 1)^2, \tag{27}$$

where z^0 is the value of z at $\eta = 0$. The integral in Eq. 27 must be evaluated numerically to obtain the value of z^0. From the expansions in Eq. 21, the values of the temperature and concentration of O_2 at $\eta = 0$ are given by

$$\left.\begin{aligned} &T^0 = T_b - \varepsilon(T_c - T_u)z^0,\\ &X_{O_2}^0 = \varepsilon\,\mathrm{Le}_{O_2}(a+z^0)/q. \end{aligned}\right\} \tag{28}$$

To calculate the leading order value of X_{H_2} at the inner layer, which is required for calculating the burning velocity, the thin sublayer within the oxidation layer, where the overall reaction II is not in equilibrium, must be analyzed. This sublayer is a transition layer in which the overall reaction II attains partial equilibrium from nonequilibrium in the inner layer. Because O_2 does not participate in step II, the quantity $X^0_{O_2}$ shown in Eq. 28 is the leading order value of X_{O_2} at the inner layer. The leading order value of temperature at the inner layer is also given by Eq. 28 because the heat release in step II is negligible.

The details of the analysis of the nonequilibrium layer are given elsewhere [1–3], therefore only the results of these previous analyses are shown here. The leading order value of X_{H_2} at the nonequilibrium layer deduced from Eq. 21 is $2\varepsilon \mathrm{Le}_{H_2}(b + z^0)/[q(1 + \alpha)]$. In the nonequilibrium layer the influence of reactions III can be neglected and reactions Ia and Ib do not take place. The expansions

$$\left.\begin{aligned} x &= \nu\bar{\zeta}, \\ X_{H_2} &= 2\varepsilon\, \mathrm{Le}_{H_2}\,(b + z^0)/[q(1 + \alpha)] + \nu\, \mathrm{Le}_{H_2}\,\tilde{z}_{H_2}, \\ X_{CO} &= 2\alpha\varepsilon\, \mathrm{Le}_{CO}\,(b + z^0)/[q(1 + \alpha)] \\ &\quad + \nu\, \mathrm{Le}_{CO}\,\tilde{z}_{CO} \end{aligned}\right\} \tag{29}$$

are introduced, where ν is a small expansion parameter and $\bar{\zeta}$, $\tilde{z}_{H_2}$, and $\tilde{z}_{CO}$ are treated as being of the order of unity. The small expansion parameter is [1–3],

$$\nu = \frac{2^{0.5}\varepsilon^{1.5}(k^0_5 C^0_M K^0_3\, \mathrm{Le}_{H_2}\, \mathrm{Le}_{O_2})^{0.5}}{q^{1.5}[(1 + \alpha)k^0_{18f} X_{H_2Ob}\, \mathrm{Le}_{CO}]^{0.5}(a + z^0)^{0.25}(b + z^0)^{0.25}}. \tag{30}$$

Following previous methods [1–3], it can be shown that $\tilde{z}_{H_2}$ and $\tilde{z}_{CO}$ are given by

$$\left.\begin{aligned} \tilde{z}_{H_2} &= -\frac{1 - \alpha}{(1 + \alpha)^{1.5}} \exp\,[-(1 + \alpha)^{0.5}\tilde{\zeta}] - \frac{2\tilde{\zeta}}{1 + \alpha}, \\ \tilde{z}CO &= \frac{1 - \alpha}{(1 + \alpha)^{1.5}} \exp\,[-(1 + \alpha)^{0.5}\tilde{\zeta}] - \frac{2\alpha\tilde{\zeta}}{1 + \alpha}. \end{aligned}\right\} \tag{31}$$

At the inner layer where $\bar{\zeta} = 0$, the value of $X^0_{H_2}$ obtained from Eqs. 21, 29, and 31 is

$$X^0_{H_2} = \frac{2\varepsilon\, \mathrm{Le}_{H_2}\,(b + z^0)}{q(1 + \alpha)} \cdot \left[1 - \frac{\nu q(1 - \alpha)}{2\varepsilon(b + z^0)(1 + \alpha)^{0.5}}\right] \tag{32}$$

The boundary condition at $\eta = 0$ given by Eq. 26 is obtained by neglecting the influence of the global step III in the inner layer and using a coupling relation among X_F, X_{CH_3}, and X_{O_2}. A different boundary condition will be obtained if the coupling relation $d^2(2X_F/\mathrm{Le}_F + 2.5X_{CH_3}/\mathrm{Le}_{CH_3} + X_{H_2}/\mathrm{Le}_{H_2} + X_{CO}/\mathrm{Le}_{CO})/dx^2 = 0$ in the inner layer, obtained from Eq. 3 after neglecting the reaction rate of global step III, is used. Integrating this coupling relation once, and matching the result with the profile for X_F in the preheat zone given by Eq. 6, gives the result $d(2X_F/\mathrm{Le}_F + 2.5X_{CH_3}/\mathrm{Le}_{CH_3} + X_{H_2}/\mathrm{Le}_{H_2} + X_{CO}/\mathrm{Le}_{CO})/dx^2 = -2$. Matching this result with the expansion for X_{H_2} and X_{CO} in Eq. 21 gives the result that $dz/d\eta$ is equal to -1 at $\eta = 0$. For stoichiometric mixtures $X_{O_2u} = 2$, therefore both coupling relations give the same result. For nonstoichiometric mixtures the value for $dz/d\eta$ obtained from integrating the coupling relation among X_F, X_{CH_3}, X_{H_2}, and X_{CO} is different from that shown in Eq. 26. The difference arises from the neglect of the global step III in the inner layer. If this step is not neglected in the inner layer, then the jump conditions can only be obtained from numerical integration of the differential equations governing the structure of this layer. For rich flames the structure of the oxidation layer can be expected to be influenced more by the consumption of O_2 and less by the oxidation of H_2 and CO, therefore the boundary condition Eq. 26 is used here. For stoichiometric and lean flames, the concentration of O_2 in the reaction zone is larger than that in rich flames. Hence, the structure of the oxidation layer of lean flames can be expected to be influenced more by the oxidation of H_2 and CO and less by the consumption of O_2. The previous asymptotic analyses of the structure of the oxidation layer of stoichiometric and lean

flames employed the boundary condition deduced from the coupling relation among the fuel, hydrogen, and carbon monoxide [1–6]. There are significant differences in the values of the burning velocities calculated using these different boundary conditions for $dz/d\eta$ at $\eta = 0$.

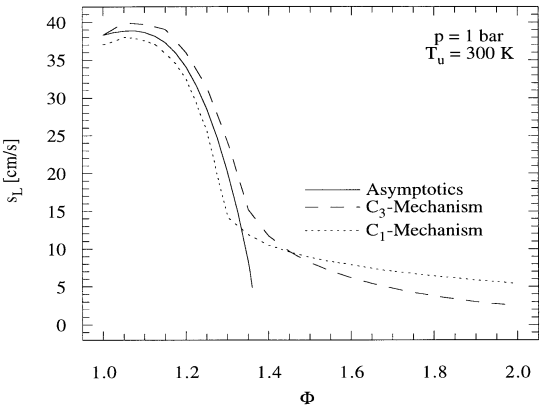

Fig. 4. Burning velocities s_L (cm/s) as functions of equivalence ratio ϕ calculated for $p = 1$ bar and $T_u = 300$ K. Solid line represents results of asymptotic analysis; dashed and dotted lines represent results of numerical calculations using the C_3-mechanism and C_1-mechanism, respectively.

BURNING VELOCITY

To calculate the value of the characteristic temperature at the inner layer T^0, it is convenient to first eliminate the quantity A appearing in the definition of L in Eq. 16 by combining it with Eq. 23. Using Eqs. 13, 24, 28, and 32 the result

$$L = \frac{2^{2.5}(k_{1f}^0)^2 k_{34}^0 (K_2^0 \,\mathrm{Le}_{\mathrm{H}_2}\,\mathrm{Le}_{\mathrm{O}_2})^{0.5}(\alpha + z^0)^2(b + z^0)^2}{k_5^0 C_M^0 k_{35}^0 k_{38}^0 (K_1^0)^{0.5}(1+\alpha)^{0.5}\,\mathrm{Le}_{\mathrm{F}}}\left[1 - \frac{\nu q(1-\alpha)}{2\varepsilon(b+z^0)(1+\alpha)^{0.5}}\right]^2 \tag{33}$$

is obtained. The right side of Eq. 33 is a function of T^0, z^0, ε, and ν. Using Eq. 28, ε can be written as a function of T^0 and z^0, and using Eq. 30 ν can be written as a function of T^0 and z^0. The quantity z^0 is given by the numerical evaluation of Eq. 27. Therefore the right side of Eq. 33 can be expressed as a function of T^0. The value of T^0 is calculated by equating the right side of Eq. 33 to the right side of Eq. 17. The quantity σ^0 appearing on the right side of Eq. 17 is given by

$$\sigma^0 = \frac{2^{1.5}k_{34}^0}{k_{35}^0}\left[\frac{K_2^0\,\mathrm{Le}_{\mathrm{H}_2}(b+z^0)}{K_1^0\,\mathrm{Le}_{\mathrm{O}_2}(a+z^0)(1+\alpha)}\right]^{0.5} \cdot \left[1 - \frac{\nu q(1-\alpha)}{2\varepsilon(b+z^0)(1+\alpha)^{0.5}}\right]^{0.5} \tag{34}$$

Equations 11, 28, and 32 are used to derive Eq. 34. To calculate the burning velocity, the second expression in Eq. 16 and Eqs. 24 and 28 are used to rewrite Eq. 23 as

$$s_L^2 = \frac{Y_{\mathrm{Fu}}}{W_{\mathrm{F}}}\left(\frac{\lambda^0}{c_p^0}\right)\left(\frac{T_u}{T^0}\right)^2 \frac{2^{1.5}k_5^0 C_M^0 (K_1^0 K_2^0)^{0.5} K_3^0\,\mathrm{Le}_{\mathrm{H}_2}^{1.5}\,\mathrm{Le}_{\mathrm{O}_2}^{1.5}}{(1+\alpha)^{1.5} q^4 X_{\mathrm{H_2Ob}} (z^0)^4}\left(\frac{T_b - T^0}{T_c - T_u}\right)^4. \tag{35}$$

RESULTS AND DISCUSSION

To calculate the burning velocities, the value of (λ^0/c_p^0) appearing in Eq. 35 is calculated using the expression $(\lambda^0/c_p^0) = 2.58 \times 10^{-5}(T^0/298)^{0.7}$ kg/(m s) [8]. The values of Le_i used in the calculations are $\mathrm{Le}_{\mathrm{F}} = \mathrm{Le}_{\mathrm{CH}_3} = 0.97$, $\mathrm{Le}_{\mathrm{O}_2} = 1.1$, $\mathrm{Le}_{\mathrm{CO}} = 1.11$, and $\mathrm{Le}_{\mathrm{H}_2} = 0.3$. The average molecular weight $\bar{W}$ is taken to be a constant and it is evaluated in the postflame zone. The values of Y_i appearing in the definition of C_M^0 also are evaluated in the postflame zone. Calculations are performed for values of ϕ equal to and greater than unity, for values of p equal to and greater than 1 bar and for various values of the initial temperature of the reactant stream T_u.

Figures 2, 4, 5, and 6 show results of calculations for $p = 1$ bar, and $T_u = 300$ K. In Fig. 4 the asymptotic results for the burning velocities, calculated as a function of the equivalence ratio ϕ, are compared with numerical results obtained using the C_3-mechanism and the C_1-mechanism. The burning velocities calculated using the C_1-mechanism agree reasonably well with those calculated using the C_3-mechanism.

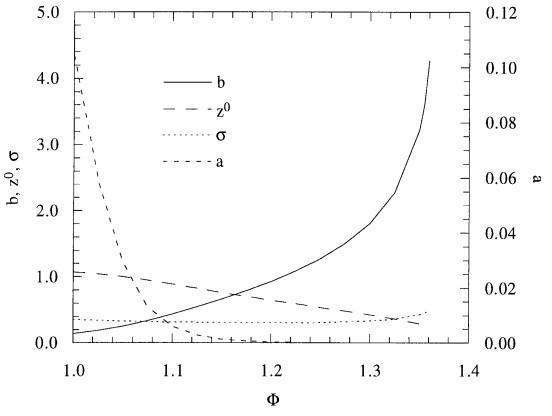

Fig. 5. Values of a, b (Eq. 21), z^0 (Eq. 27), and σ^0 (Eq. 11) as functions of equivalence ratio ϕ calculated for $p = 1$ bar and $T_u = 300$ K.

For ϕ slightly larger than unity and less than 1.36, the numerical results show s_L to decrease rapidly with increasing equivalence ratio. For ϕ larger than 1.36 the numerical results show s_L to decrease more slowly with increasing equivalence ratios. For ϕ less than 1.36, Fig. 4 shows the values of s_L calculated using the C_3-mechanism to be larger than those calculated using the C_1-mechanism. This is attributed to the larger overall chain-breaking effects in the C_1-mechanism in comparison with those in the C_3-mechanism. This is consistent with previous numerical results that show the burning velocities calculated using the C_2-mechanism to be higher than those calculated using the C_1-mechanism [10]. Figure 4 shows the asymptotic results for the burning velocities to agree quite well with the numerical results for $\phi < 1.36$. The asymptotic analysis did not give converged solutions for equivalence ratios greater than 1.36. At $\phi = 1.36$, the asymptotic result for s_L is 4.95 cm/s.

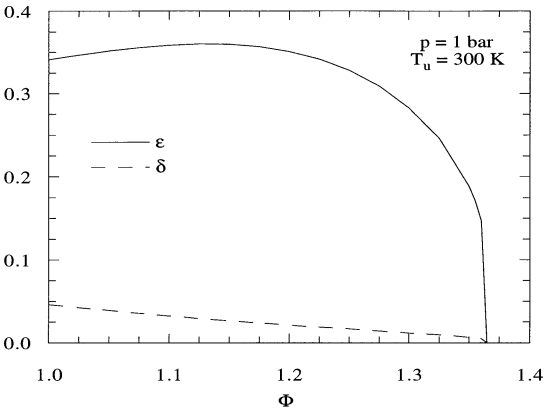

Fig. 6. Characteristic nondimensional thickness of inner layer δ and oxidation layer ε, as functions of the equivalence ratio ϕ calculated for $p = 1$ bar and $T_u = 300$ K.

Figure 2 shows values of T_c, T_b, and T^0 as functions of ϕ. With increasing ϕ, the values of T_c and T_b decrease and the values of T^0 increase. This trend is similar to previous asymptotic results for lean flames where the values of T^0 also increased with increasing ϕ [1–6]. Figure 2 shows T^0 to approach T_b as ϕ increases. Equation 35 shows that the burning velocity is proportional to the fourth power of the difference between T_b and T^0. With increasing values of the equivalence ratio this difference decreases, which contributes to the decrease in the values of s_L shown in Fig. 4. Equation 21 shows that the difference between τ_b and τ^0 is of order ε. With increasing values of ϕ as T^0 approaches T_b, the difference between τ_b and τ^0 decreases. When this difference is of order δ, the asymptotic analysis developed here does not apply. At these conditions an alternative analysis must be developed to predict the slow decrease in s_L with increasing ϕ as shown by the numerical results in Fig. 4.

Figure 5 shows values of a, b (Eq. 21), z^0 (Eq. 27), and σ^0 (Eq. 11) as functions of ϕ. With increasing ϕ, there is a sharp decrease in the values of a and a sharp increase in the values of b. Thus in the postflame zone with increasing values of the equivalence ratio, the equilibrium concentration of O_2 decreases and the equilibrium concentration of H_2 increases. The parameter σ^0 is a weak function of ϕ.

Figure 6 shows values of the characteristic nondimensional thickness of the inner layer δ, and the oxidation layer ε, as functions of the equivalence ratio ϕ. The results show that the presumed ordering $\delta \ll \varepsilon \ll 1$ is maintained. The values of δ slowly decrease with increasing ϕ. The values of ε first slowly increase with increasing ϕ and then rapidly decrease and approach δ. When the values of δ and ε become equal, the inner layer and the oxidation layer merge and the asymptotic analysis developed here is no longer valid. This implies that for very rich flames an alternative asymptotic analysis

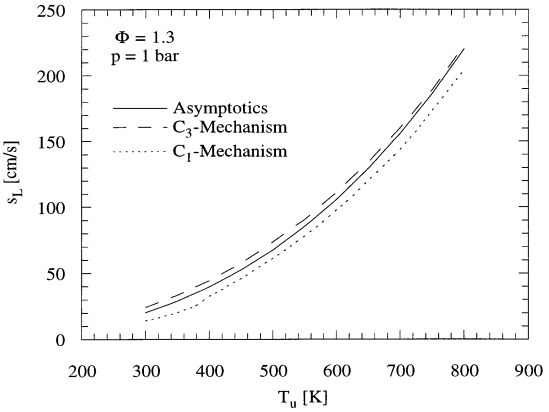

Fig. 7. Burning velocities s_L (cm/s) as functions of initial temperature of reactants T_u calculated for $\phi = 1.3$ and $p = 1$ bar. Solid line represents results of asymptotic analysis, dashed and dotted lines represent results of numerical calculations performed using C_3-mechanism and C_1-mechanism, respectively.

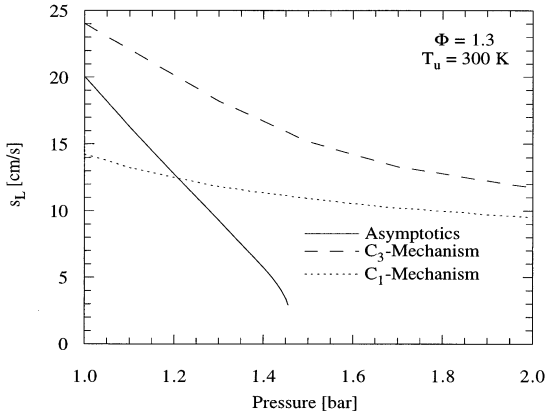

Fig. 8. Burning velocities s_L, (cm/s) as functions of pressure p (bars) calculated for $\phi = 1.3$ and $T_u = 300$ K. Solid line represents results of asymptotic analysis, dashed and dotted lines represent results of numerical calculations performed using C_3-mechanism and C_1-mechanism, respectively.

must be developed, in which all reactions are presumed to take place in one layer.

The analysis developed here is valid for moderately rich flames. Therefore further tests of the predictions of the asymptotic model are made at $\phi = 1.3$. In Fig. 7 the burning velocities, calculated using the results of asymptotic analysis for $\phi = 1.3$, $p = 1$ bar, and for various values of the initial temperature of the reactant stream are compared with numerical results obtained using the C_3-mechanism and the C_1-mechanism. At $p = 1$ bar and $T_u = 300$ K, the value of s_L calculated using results of asymptotic analysis is 20.07 cm/s, which is smaller than the numerical result 24.05 cm/s obtained using the C_3-mechanism and larger than the numerical result 14.21 cm/s obtained using the C_1-mechanism. Figure 7 show the asymptotic results to agree well with the numerical results. In Fig. 8 the burning velocities, calculated using the results of asymptotic analysis for $\phi = 1.3$, $T_u = 300$ K, and for various values of the pressure, are compared with numerical results obtained using the C_3-mechanism and the C_1-mechanism. For increasing values of p, Fig. 8 shows the asymptotic results for s_L to decrease much more rapidly than the numerical results. The asymptotic analysis did not give converged solutions for pressures greater than 1.455 bars.

SUMMARY AND CONCLUSIONS

An asymptotic analysis of the structure of moderately rich methane flames has been described. The analysis employs a reduced four-step chemical-kinetic mechanism. This differs from those employed in previous asymptotic analyses of stoichiometric and lean methane flames [1–6], because a steady-state approximation is not introduced for CH_3. The results of the asymptotic analysis show the burning velocities s_L to decrease rapidly with increasing equivalence ratio. This is in agreement with results of numerical calculations obtained using chemical-kinetic mechanisms made up of elementary reactions. Previous asymptotic analyses of stoichiometric and lean methane flames did not predict this rapid decrease in the values of the burning velocities for rich flames [1–6].

In the asymptotic analysis developed here chemical reactions are presumed to take place in two layers, the inner layer and the oxidation layer. This is similar to previous asymptotic analyses of stoichiometric and lean flames [1–6]. In these previous analyses the rate determining reactions taking place in the inner layer were presumed to be between the fuel and radicals (H and OH). In the inner layer of rich flames, in addition to these reactions, the reaction between CH_3 and O atoms given by step 35 (see Table 1) also has a rate determining influ-

ence on the structure of this layer. The influence of this reaction in rich flames, in comparison with those in lean flames, arises from the lower level of O atoms. Also, the enhanced influence of the chain-breaking reaction 34 in rich flames, in comparison with that in lean flames, decreases the concentration of H radicals, which in turn decreases the values of the burning velocities. The success of the present analysis, in predicting the observed rapid decrease in the values of the burning velocities with increasing equivalence ratio, for moderately rich flames is attributed to the influence of reaction 34 on the structure of the inner layer. The structure of the oxidation layer of rich flames is influenced mainly by the consumption of O_2, whereas for lean flames the structure of this layer is influenced mainly by the oxidation of hydrogen and carbon monoxide.

The asymptotic analysis developed here applies to moderately rich flames. At values of the equivalence ratio larger than 1.36, all chemical reactions will take place in one layer with $T^0 = T_b$. Asymptotic analyses of these rich flames are yet to be developed.

The authors thank M. Bollig for providing numerical results that were used to develop the asymptotic analysis. The research was supported by the U.S. Army Research Office Grant # ARO DAAH-95-1-0108.

REFERENCES

1. Peters, N., and Williams, F. A., *Combust. Flame* 68: 185–207 (1987).
2. Seshadri, K., and Peters, N., *Combust. Flame*, 81:96–118 (1990).
3. Seshadri, K., and Göttgens, J., *Reduced Kinetic Mechanisms and Asymptotic Approximations for Methane-Air Flames*, (M. D. Smooke, Ed.) Vol. 384 of *Lecture Notes in Physics*, Springer-Verlag, Berlin, 1991, pp. 111–136.
4. Bui-Pham, M., Seshadri, K., and Williams, F. A., *Combust. Flame*, 89:343–362 (1992).
5. Seshadri, K., and Williams, F. A., in *Turbulent Reacting Flows*, (P. A. Libby and F. A. Williams, Eds.), Academic Press, San Diego, CA, 1994, pp. 153–210.
6. Seshadri, K., *Twenty-Sixth Symposium (International) on Combustion*, The Combustion Institute, Pittsburgh, 1996, pp. 831–846.
7. Smooke, M. D., and Giovangigli, V., in *Reduced Kinetic Mechanisms and Asymptotic Approximations for Methane-Air Flames*, (M. D. Smooke, Ed.), Vol. 384 of *Lecture Notes in Physics*, Springer-Verlag, Berlin, 1991, pp. 1–28.
8. Smooke, M. D., and Giovangigli, V., in *Reduced Kinetic Mechanisms and Asymptotic Approximations for Methane-Air Flames*, (M. D. Smooke, Ed.), Vol. 384 of *Lecture Notes in Physics*, Springer-Verlag, Berlin, 1991, pp. 29–47.
9. Peters, N., in *Reduced Kinetic Mechanisms and Asymptotic Approximations for Methane-Air Flames*, (M. D. Smooke, ed.), Vol. 384 of *Lecture Notes in Physics*, Springer-Verlag, Berlin, 1991, pp. 48–67.
10. Mauß, F., and Peters, N., in *Reduced Kinetic Mechanisms for Applications in Combustion Systems*, (N. Peters and B. Rogg, eds.), Vol. m15 of *Lecture Notes in Physics*, Springer-Verlag, Berlin, 1993, pp. 58–75.
11. Peters, N., and Rogg, B., Eds., *Reduced Kinetic Mechanisms for Application in Combustion Systems*, Vol. m15 of *Lecture Notes in Physics*, Springer-Verlag, Heidelberg, 1993 p. 8–12.
12. Chelliah, H. K., Seshadri, K., and Law, C. K., in *Reduced Kinetic Mechanisms for Applications in Combustion Systems*, (N. Peters and B. Rogg, Eds.), Vol. m15 of *Lecture Notes in Physics*, Springer-Verlag, Berlin, 1993, pp. 224–240.
13. Williams, F. A., *Combustion Theory*, 2nd ed., Addison-Wesley Publishing Company, Redwood City, CA, 1985 p. 11.
14. Williams, F. A., in *Modern Developments in Propulsion and Combustion*, Chap. 4 (G. D. Roy, Ed.), Taylor & Francis, Wasgington, D.C. 1996.

Received 28 October 1996; accepted 5 August 1997